OPTOELECTRONICS AND ADVANCED MATERIALS – RAPID COMMUNICATIONS Vol. 14, No. 11-12, November-December 2020, p. 501-508

An active sensor imaging for dense target environments

R. F. CINAR, A. DEMIRKOL*
Electrical - Electronics Engineering Department, Sakarya University, Sakarya, 54050, Turkey

Target density functions are the fundamental tools that map the reflectivity distribution by processing backscatter radar data. Radar imaging systems frequently employ these forms of functions to extract meaningful data from more complicated signal space. In this paper, an outline and a coherent reconstruction method for a newly defined target density function for radar imaging are presented. The studied approach is based on the fact that the geometry of the radar processing benefits from angular scanning along the cross-range. The proposed frame is available to be used with phased array radar systems as well as applied to various radar problems. Hypothetical background and step-by-step derivation of the mathematical model are discussed. Comparison with other conventional radar imaging methods and strength of the new method is emphasized, an implementation using simulated unprocessed data is achieved, outcomes are discussed in terms of benefits and finally the future work is given. The results promise simplicity and speed, as well as providing a new method to radar imaging.

(Received June 22, 2020; accepted November 25, 2020)

Keywords: Phased Array Radar, Radar Imaging, Reflectivity Functions, SAR - ISAR, Target Density Functions

1. Introduction

The idea of imaging with radar is basically mapping the reflectivity of the target scene upon a spatial representation, but the reason that makes radar imaging advantageous is the use of electromagnetic radio waves. Besides the radio waves being able to detect from long distances, it has dominance over optical imaging systems since it is immune to natural obstacles such as high opacity and low light environment. The ability to obtain more specific information with polarization and phase from the target area makes radar an important instrument for imaging in various problems [1]–[4].

The concept of target density functions referred to by different names are fundamental tools widely used in radar problems; additionally, radar problems become target density function problems after composing the mathematical representation of the given signal space. The main aim to process the target density/reflectivity function from an acquired data is to discriminate the target signature at the correct position on signal collection [5].

2. Preliminaries to the study

The first "target density" definition was used by Fowle et al. in a pioneer study on radar performance analysis in a dense target environment in 1961 [6]. This approach was comprising a target density definition, based on a special function, an ambiguity function form primarily developed by Woodward [7] which has two variables: range, and velocity. The defined function $\chi(\cdot)$ is:

$$\chi(\tau, v) = \frac{1}{2E}\int_{-\infty}^{\infty} \mu(t)\mu^*(t-\tau)e^{-j2\pi vt}\,dt \quad (1)$$

where E is the total energy of the signal and $\mu(t)$ is the complex modulation function of the signal. In this equation, τ is the time difference between target's actual delay and the delay belonging to any portion of the signal, whereas v is the difference between the actual Doppler shift of the target and the Doppler shift match point of the receiver's matched filter. Thus, the theory considers the target signature as a sum of these two-dimensional delay-Doppler distribution collections of a single target inside a dense clutter environment [6]. It is used to emphasize to define complex targets and separate the single and multiple targets. Rihaczek theoretically extended this approach to fill the gaps for pulse trains and reach satisfying resolution qualities in the following works [8], [9]. Following studies from Rihaczek and Spafford discussed the effects of the signal design, moving target, and multiple target environments on target density [10], [11].

In another study [12], Naparst advances the theory of Fowle for a new approach as well as the first use of the "target density function" term. Briefly, the hypothetical statement of the method used by Naparst is:

$$\langle e_n, s_m\rangle = \int_0^{\infty}\int_{-\infty}^{\infty} D(x,y) \times \sqrt{y}\int_{-\infty}^{\infty} s_n\big((t-x)\big)\overline{s_m}(t)\,dt\,dx\,dy \quad (2)$$

by narrowing to a more compact representation:

$$\langle e_n, s_m\rangle = \int_0^{\infty}\int_{-\infty}^{\infty} D(x,y) \times A_{n,m}(x,y)\,dx\,dy \quad (3)$$

where $\langle e_n, s_m \rangle$ term is the inner product of the transmitted and received signals, $D(x,y)$ is the target density function and $A(\cdot)$ is the wideband cross-ambiguity function. Two deterministic solutions of (3) are proposed in [12], in order to expand the target density function toward the sum of cross-ambiguity functions. The final case yields the solution as can be seen in (4), clearly expressing the decomposition,

$$D(x,y) \approx \frac{1}{\sqrt{y}} \sum_{n,m=0}^{\infty} c_{nm}\, A_{nm}(x,y) \tag{4}$$

where c_{nm} is the constant that represents the infinite integration of the inner product of transmitted and received signals from the point (n,m) within the target scene.

After the development of the modern synthetic aperture techniques, more advanced approaches have started to take place in radar imaging literature. One of the most common usages of target functions synthesizing images from phase history can be seen in the conventional Synthetic Aperture Radar and Inverse Synthetic Aperture Radar (SAR - ISAR) approaches. Both approaches have the same mathematical background, but the geometric formations are different owing to the difference between the relative movements of the target and the array.

Let consider an ideal target that has a complex cross-section of σ_t at the position of (x,y,z), then the received signal is delayed and attenuated version of the transmitted signal. The three-dimensional signal model of the backscatter can be expressed as:

$$s_R(t) = \int_{-\infty}^{\infty}\int_{-\infty}^{\infty}\int_{-\infty}^{\infty} \rho(x,y,z) \times exp\left(-j2\pi f_0 \frac{2R_p(t)}{c}\right) dx\, dy\, dz \tag{5}$$

for the conditions that regulate the limit between range as a function time and pulse repetition interval time:

$$2R_p(t)/c \le t \le T_{PRI} + 2R_p(t)/c \tag{6}$$

Here, $\rho = \sqrt{\sigma_t}$ is the average reflectivity coefficients along the voxel at the position (x,y,z), T_{PRI} is the pulse repetition time interval and f_0 is the center frequency. $R_p(t)$ is the expression of range function, changing with time and angular motion. With an expanded approximate expression:

$$R_p(t) \cong R(t) + x\cos[a(t)-\theta] - y\sin[a(t)-\theta] \tag{7}$$

Some simplifications can be made by taking advantage of assumes and omissions. Coherent reconstruction of the frequency-dependent reflectivity function $\rho(x,y,z)$ on a two-dimensional plane by compensating the motion errors and phase distortions produced by the complex motion of target is called SAR-ISAR image formation [13]–[16].

Several different algorithms are developed for SAR-ISAR reconstruction; Radon transform-based back-projection algorithm [17], [18], range stack algorithm [19], $omega - k$ algorithm [20], time-frequency based spectral approaches that benefit from processing in informative domains [13], time-domain correlation (TDC) [21] and polar reformat algorithm based on tomographic imaging techniques [22] can be demonstrated among the most commonly used ones. Individually, these algorithms have powerful and weak sides on some matters such as processual cost, maneuvering target problems, multiple target problems, reliability against focal errors, low or high scanning angle, and algorithmic complexity.

3. Imaging with Target Density Functions

3.1. Reflectivity and dense target environment

The expectation from a radar imaging system is to distinguish the impulse response or the point spread functions (PSF) of the close elementary targets. Here, the target signature can be assumed as a composition of point-like pulses, ideally a combination of perfect delta-Dirac functions, but practically, it spreads to functions like sinc due to the signal acquisition under finite bandwidth.

The more enhancement of the resolution means achieving the more detailed mapping of these structures. One more point to be remarked is that imaging systems have more than one dimension that spread the impulse response of the target signature. A reason for this spread is the continuous illumination of the scatter points of the target, during the formation process [23]. One other reason is the targets with higher dimensions that invade larger area, maybe more than a few points on the image, cause interactions with the impulse response distributions of the small targets. Thus, an exact definition of resolution cannot be made instead of theoretical assumptions. Surely, despite the necessity of high resolution that forces one to use narrower pulses, the trade-offs between resolution, total pulse energy, efficiency of the transmission, and activity of the physical circuits should be examined carefully. Other phenomenal effects such as multipath and clutter are well worked already and can be found in radar literature [1], [2].

Range resolution (ρ_r) gets improved when the transmitted waveform bandwidth (B) is larger, whereas azimuth resolution (ρ_a) is better if the active effective size of the phased array (A_e) is bigger and it occurs as the synthetic aperture length increases [24], expressively:

$$\rho_r = \frac{c}{2B} \tag{8}$$

where B is the bandwidth and c is the propagation speed of the transmitted signal.

For determination of the cross-range resolution, the angular resolution (ρ_θ) must be defined first:

$$\rho_\theta = {}^{\lambda}/_{2A_e} = \frac{\lambda}{2(M_t M_r - 1)d \cdot \cos\theta} \quad (9)$$

where θ is the aspect angle, d is array spacing, M_t is the number of transmitter elements and M_r is the number of the receiver elements. Thus, the cross-range resolution (δR) belongs to a position with parameters θ and R becomes approximately [25]:

$$\delta R \approx \rho_\theta \cdot R \quad (10)$$

3.2. Imaging model

Let suppose a phased array antenna is composed of N identical elements with linear and symmetrical distribution with a range of $-x$ to x, for x equals to $(N-1)/2 \cdot d$ and $-x$ equals to $-(N-1)/2 \cdot d$, where d is spacing of the antenna elements. To adjust the direction of the beam pattern around the interested target scene, a compact linear phase form for i^{th} antenna element is formulated below:

$$exp\left(-j\frac{2\pi}{\lambda}x_i \cdot \cos(\theta)\right) \quad (11)$$

where the angle of steering is represented by θ, wavelength by λ and i is the indices for the initial element in the steering process [26], [27]. Thus, a focused beam, with angle θ is achieved on the radiational far-field region by manipulating the phases of the excitation signals on entire radiating elements. The rationale behind the usage of the phased array is to take advantage of the same steerable pattern, i.e. bi-directional behavior in sending and receiving. In many applications, both sending and receiving systems are separately required as bistatic radar; the solution to this problem is known as the compact transmit/receive module (T-R module). Phased array systems usually employ the individual antenna elements with a spacing of half of the signal wavelength; surely, some other formations with different goals are used as well. In this work, the gain of the array can be considered uniform for all scanning directions, for simplicity [26], [27].

Let start with the definition of the transmitted signal; consider $p(t)$, a periodic function of time, such as pulse train shown below for $\omega_0 = 2\pi \times PRF$:

$$p(t) = \sum_{k=-\infty}^{\infty} a_k e^{jk\omega_0 t} \quad (12)$$

where a_k is the amplitude for harmonic number k and PRF is the pulse repetition frequency. For a typical narrow band radar, a stepped frequency or a chirp waveform can provide high range resolution [28].

Before the transmission, we multiply the radar waveform $p(t)$ by a carrier wave $s_c(t)$ to get the modulated signal $s_m(t)$ as follows:

$$s_m(t) = p(t) \times s_c(t) \quad (13)$$

where the carrier signal is a sinusoidal waveform with higher frequency as follows:

$$s_c(t) = e^{jk\omega_c t} \quad (14)$$

Let consider the area imaged within the desired limits, $R \in [R_c - R_0\,,\ R_c + R_0]$ along the slant range and $\theta \in [\theta_c - \theta_0\,,\ \theta_c + \theta_0]$ along the scanning angle by considering the symmetric approach for the target area where θ_c is the center of the angular domain and R_c is assumed center of the target area along the range. For a single scatter point at the position (R, β), representation of the reflectivity is:

$$y(x,t) = s_m\left(t - {}^{2R}/_{c} - {}^{\beta x}/_{c}\right) g(R,\beta) \quad (15)$$

where x is the dimension of the actual element of the array and t is the time. Here, it can be remarked that the $y(\cdot)$ is a back-reflected and delayed replica of the modulated signal $s_m(t)$ from the point (R, β). It should be emphasized that the target density function, $g(R, \beta)$, that this paper giving a point on has a unique pair of spatial definition, (R, β), where R is the radial range and the β is the angular cosine, i.e. the cosine of the scanning angle θ. The imaging geometry of the target scene can be seen in Fig. 1.

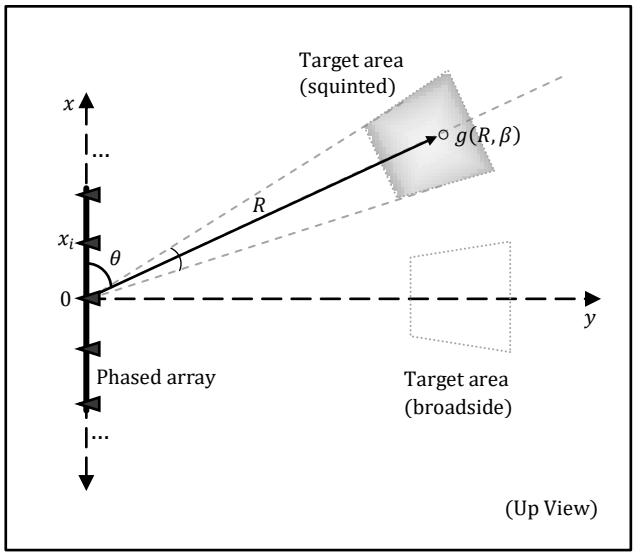

Fig. 1. Imaging scenario and geometry

In literature, radar imaging methods express the target model as mapping of the reflective points on a spatial plane. By considering whole the imaging plane within boundaries, superposition of the amplitude and phase representation of all the reflective points can be shown as,

$$y(x,t) = \int_{-1}^{1}\int_{R_{min}}^{R_{max}} s_m\left(t - {2R}/{c} - {\beta x}/{c}\right) \times g(R,\beta)\, dR\, d\beta \quad (16)$$

by organizing the modulated signal yields:

$$y(x,t) = \int_{-1}^{1}\int_{R_{min}}^{R_{max}} p\left(t - {2R}/{c} - {\beta x}/{c}\right) \times e^{-j\omega_c\left(t-{2R}/{c}-{\beta x}/{c}\right)} e^{-j\omega_c t} g(R,\beta)\, dR\, d\beta \quad (17)$$

where $y(x,t)$ is the output of the antenna element located at the center of the array, and c is the propagation speed of the wave, light speed for the ideal case.

This expression can be rewritten by taking the pulse train given in (12) into account:

$$y(x,t) = \sum_{k=-\infty}^{\infty} \alpha_k e^{-j(\omega_c+k\omega_0)t} \int_{-1}^{1}\int_{R_{min}}^{R_{max}} e^{-j(\omega_c+k\omega_0)({2R}/{c})} \times e^{-j(\omega_c+k\omega_0)\left({\beta x}/{c}\right)} g(R,\beta)\, dR\, d\beta \quad (18)$$

where k is the notation of the harmonics that stated before, in (12).

Next step continues by demodulation process, here the information content extracted from the carrier by multiplying $s_d(t)$ with the synthesized equation $y(x,t)$:

$$s_d(t) = e^{-j(\omega_c+k\omega_0)t} \quad (19)$$

thus the effect of the carrier is removed from the collected, raw data, the equation becomes as follows:

$$Y(k,x) = \int_{-1}^{1}\int_{R_{min}}^{R_{max}} e^{-j(\omega_c+k\omega_0)({2R}/{c})} \times e^{-j(\omega_c+k\omega_0)\left({\beta x}/{c}\right)} g(R,\beta)\, dR\, d\beta \quad (20)$$

For fixed k and β variables, target density distribution along the range becomes:

$$G(k.\beta) = \int_{R_{min}}^{R_{max}} g(R,\beta)\, e^{-j(\omega_c+k\omega_0)({2R}/{c})}\, dR \quad (21)$$

and clearly, for fixed k and x variables:

$$Y(k.x) = \int_{-1}^{1} G(k,\beta)\, e^{-j(\omega_c+k\omega_0)\left({\beta x}/{c}\right)}\, d\beta \quad (22)$$

Range resolution capabilities of the transmitted signal can be evaluated at the output of this step of the process by observing the high-resolution range profiles which has the spread of each target's signature along the R. As k in the previous equation is fixed, for notational simplicity, it can be written as follows:

$$Y_k(x) = \int_{-1}^{1} G_k(\beta)\, e^{-j(\omega_c+k\omega_0)\left({\beta x}/{c}\right)}\, d\beta \quad (23)$$

So far, all the process was handled for the single sensor at the center of the array. For N sensors that are individually linearly spaced at $x = x_i$, the output of the array for each angle becomes:

$$a_i(\beta) = e^{-j(\omega_c+k\omega_0)\left(\frac{x_i}{c}\beta\right)} \quad (24)$$

Thus, for some constant of b_i, the estimation of the $G_k(\beta)$ becomes approximately:

$$G_k(\beta) = \sum_{i=-\infty}^{\infty} b_i \times a_i(\beta) \quad (25)$$

Equation (22) and (23) show the superposition of the back reflections along the array, for a fixed incident angle, θ.

If the beamforming model stated in (24) and (25) are reorganized as anticipated, the expected target density function is finalized in form of Fourier series as below:

$$g(R,\beta) = \sum_{k=-\infty}^{\infty} G_k(\beta)\, e^{j(\omega_c+k\omega_0)({2R}/{c})} \quad (26)$$

here, the infinite limits of the array are practically impossible, thus limits are replaced with finite aperture composed of N elements by considering a symmetric approach for array processing.

$$g(R,\beta) = \sum_{k=-(N-1)/2}^{(N-1)/2} G_k(\beta)\, e^{j(\omega_c+k\omega_0)({2R}/{c})} \quad (27)$$

The resulting function with Fourier theory will make more contributions to active sensor imaging. Equation (27) is the final expression that clearly reconstructs the target density function distribution on the (R,β) plane.

4. Implementation

4.1. Technical details

The theoretical basis of the method introduced in this paper is demonstrated in a general frame. An implementation is conducted for verification of the validity of the proposed approach, for a radar operates in spotlight mode, as well as easily adapted to inverse synthetic aperture radar operations. A raw data synthesizer with high accuracy is designed to generate backscatter data from desired number of targets by computing phase change related to delays.

A radar array, consisting of nine antenna elements, one of which is in the center with a spacing of $\lambda/2$, is

considered for a fixed position and has an accurate range and direction information of the targets. Presumed targets are ideal point-like, Swerling-0 model [1], [29] that enable one to observe point spread function shape and discrimination of close targets on resulting image [30]. The preferred specifications are shown in Table 1.

Table 1. Implementation parameters

Symbol	Definition	Value
	Signal type	LFM
T	Signal duration	2.5×10^{-7} s
B	Signal bandwidth	100 MHz
f_c	Carrier frequency	500 MHz
R	Initial position in range	1000 m
PRI	Pulse Repetition Interval	20×10^{-6} s
θ_{min}	Angle (min)	Broadside (-10) deg.
θ_{max}	Angle (max)	Broadside $(+10)$ deg.
θ_{sq}	Squint angle (in squint mode)	30 deg.
N	Number of the array elements	9
d	Spacing of the array elements	$\lambda/2$
n_t	Number of the targets	5
c	lightspeed	3×10^8 m/s

LFM is the abbreviation for Linear Frequency Modulated Signal, s=second, m=meter, MHz=Mega-Hertz, deg.=degrees.

A train of LFM pulses are transmitted from the array and signal to noise ratio is set to 10 dB. Designed LFM pulse is selected symmetric by the reason of its capability of good noise immunity and production of low sidelobes levels; good accuracy in estimation of other parameters used in the imaging algorithm is one other advantage in using this waveform [31], [32]. A brief flowchart of the algorithm given above, showing the basic steps, starting with the acquisition of data up to the plot of the image, is given in Fig. 2 below.

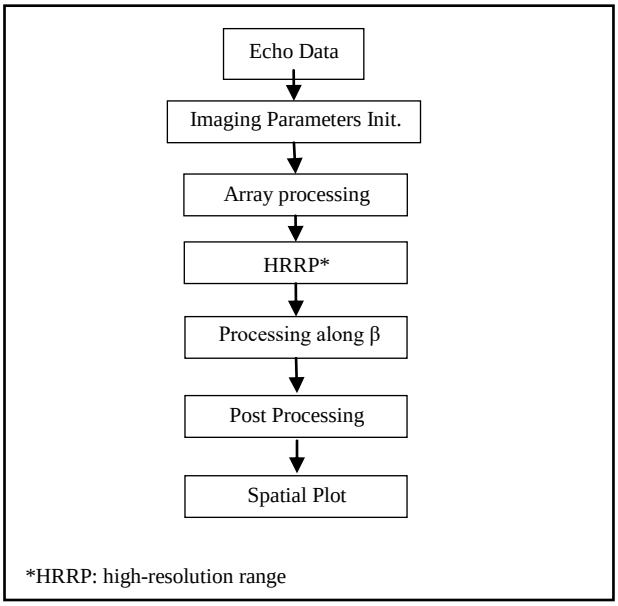

Fig. 2. Flow chart for the reconstruction of Target Density Function

4.2. Results

In this section, some results of both the method derived and the other conventional methods are presented. The same dataset is used in all algorithms to be able to compare the quality of the final images. Here, three different commonly used reconstruction algorithms are chosen for comparison as conventional radar imaging systems such as Omega-k algorithm, Range Stack algorithm, and Convolutional Back-projection algorithm.

By a majority, it is preferred to be used the algorithms not generating additional errors due to a phase approximation or digital data interpolation. Range Stacking [19] and Omega-k [20] algorithms are analyzed belong to the group of relatively modern reconstruction algorithms that do not contain focal errors. Both these approaches are classified in high-resolution radar imaging techniques; however, digital data interpolation is not required in the Range Stacking Algorithm, thus processual errors such as truncation errors are not observed.

The resulting image of the Omega-k algorithm (stated in other words Migration Algorithm or Wavefront Algorithm in some references) is demonstrated below, in Fig. 3.

The shape of the point spread function can be clearly observed around the neighborhoods of the target located at the origin of the target scene, descriptively, the spread of the target at the coordinates (1000,0) in the following images will demonstrate the response of the imaging algorithms.

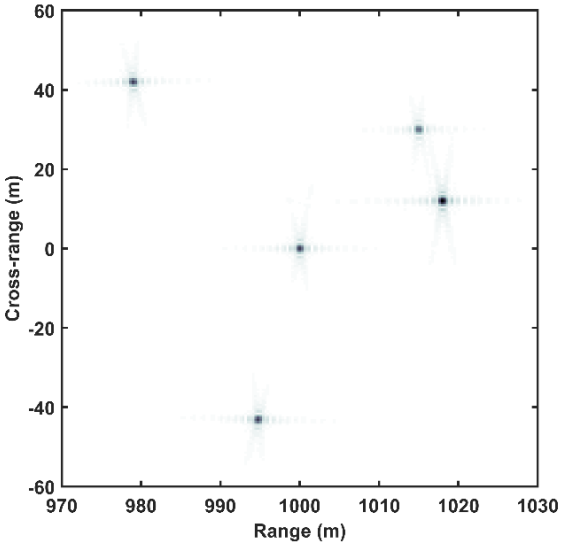

Fig. 3. SAR image reconstructed with Omega-k algorithm

The second one is the Range Stack algorithm. This algorithm continuously reforms the target function for all the range points within the imaging interval, thus it called Range Stacking [19]. Fig. 4. Shows the resulting image of the Range Stack algorithm.

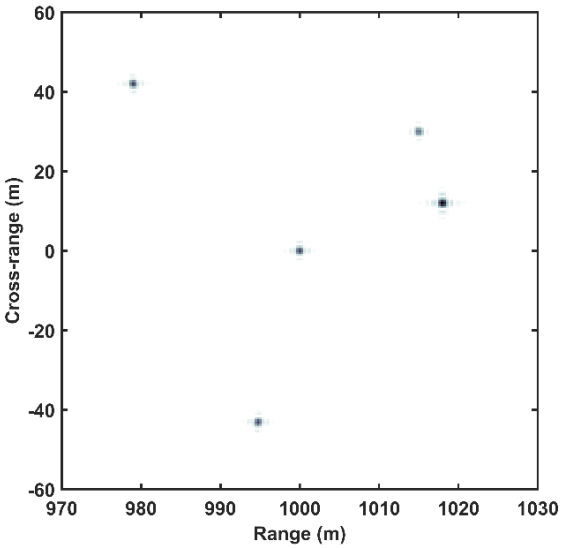

Fig. 4. SAR image reconstructed with Range Stack algorithm

One other result that can be seen in Fig. 5, is the output of the Convolutional Back-projection algorithm. The Back-projection algorithm is one of the commonly used algorithms due to its real-time running capability and applicability to wide areas, despite its poor computational efficiency [17], [18].

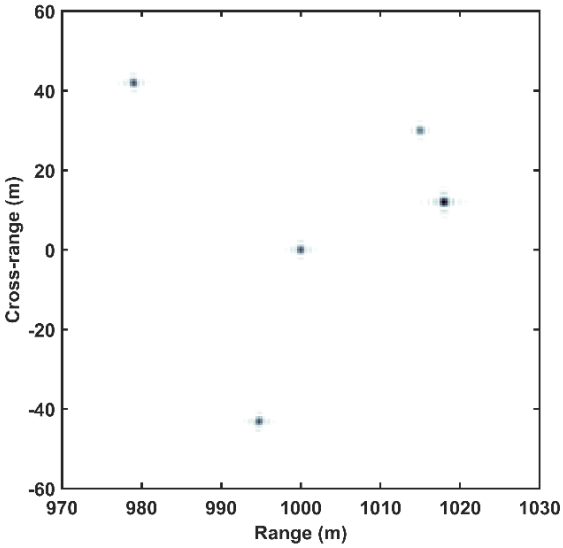

Fig. 5. SAR image reconstructed with Convolutional Back-projection Algorithm

As for the developed model in this study, the images demonstrate the results of the radar reconstruction with target density functions. Recovery around the target points is at the desired level, moreover, this result is obtained with a fast and simple algorithm. As stated previously, with higher bandwidth and angular variation, it is possible to reach better focus within the neighborhoods of the target; in other words, a peak-like point spread function closer to ideal form.

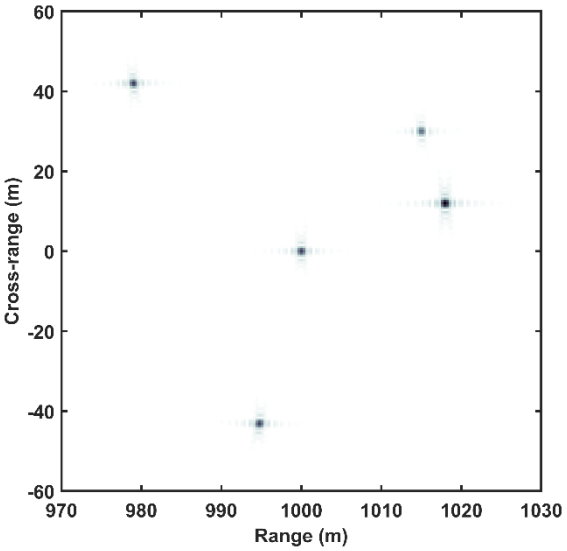

Fig. 6. Output of the algorithm stated for Target Density Function Reconstruction (broadside mode)

Total angular variation is directly related to the β, thus increased total scanning angle yields an improved image along the cross-range plane. By considering (23),

the smaller angular interval gives closer integral limits, thus the closer phase terms that limits one to distinguish the close targets along β, in other words, particularly, the close targets have same R cannot be resolved.

Next image shows the result of an imaging scenario has a squint angle of 30 degrees and ± 10 degrees of the imaging angular interval for the presented algorithm. Parameters are kept as shown in Table 1. Another advantage of the use of the angular parameter in core function appears in squint imaging. In classic SAR reconstruction algorithms, the squint process is being handled in a separated step by using baseband conversion in the slow time domain.

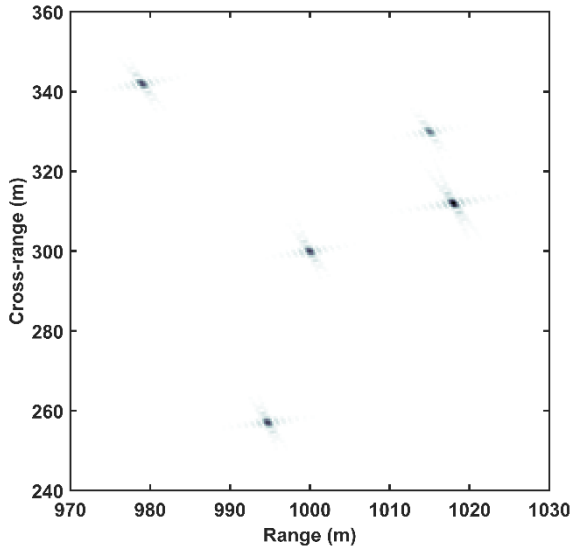

Fig. 7. Output of the algorithm stated for Target Density Function Reconstruction (squint mode with an angle of 30 degrees)

It is clear that the synthesized datasets used in this implementation are acquired from a target with a known and stable trajectory; consequently, time-consuming steps such as post-processing for image enhancement are not taken into account during the analysis of the computational processing complexity and runtime analysis, but only the reconstruction algorithms [33].

Table 2. Processual Runtimes of the Algorithms

Algorithm	Runtime
Omega-K algorithm	0.461 sec.
Range Stack algorithm	10.551 sec.
Back Projection algorithm	55.201 sec.
Reconstruction with Target Density Function	0.621 sec.

sec.: second

Table 2 indicates the comparative results of the execution time of the algorithms measured under the same computation conditions. The tool was used in the analysis of runtime statistics is Profiler under MATLAB® software. The results declare that the execution time efficiency of the introduced algorithm is acceptable; by comparing the simplicity of the algorithm with others, considerable advantageous.

Additionally, all the results are enhanced by filtering out the noise and residues of the process on the frequency domain and cross-terms are removed on the ambiguity domain.

5. Conclusion and Future Work

Target density functions are useful for the extraction of the spatial reflectivity distribution of the targets from non-processed backscatter data and motion information of the target. Determination of the point spread function of the individual targets enables one to bypass the beamforming on the receiver side.

Direct use of angular variables on imaging function makes it possible to ease the formulation of the squint process. As given in results, it is clear that the derived $g(R,\beta)$ type target density functions are successful both for the broadside and for the squinted mode imaging. Whereas, conventional approaches may require more complicated squint process steps, $g(R,\beta)$ is practically based upon Fourier theory.

The complexity of the derived method is discussed and compared with other methods; practicality of the new method provides an insight into the convenience of use. Processual cost-efficiency of the method is examined by comparing other chosen methods. Results obtained from the runtime analysis are presented in Table 2 and confirm that the processual cost-efficiency is one other powerful side of the algorithm proposed.

In future works, this theoretical formation is planned to be expanded for a wideband approach and a new formation will be put forward by considering the physical challenges for wideband imaging applications, such as through-the-wall and in-wall radar imaging.

Acknowledgement

This work has been supported by Sakarya University Scientific Research Projects Coordination Unit under grant number 2017-50-02-019.

References

[1] M. I. Skolnik, Introduction to radar systems, McGraw Hill, 2001.
[2] M. I. Skolnik, Radar Handbook, 2008.
[3] Habibur, Rahman, Fundamental Principles of Radar, CRC Press LLC, 2019.
[4] W. Emery and A. Camps, Introduction to satellite

remote sensing: Atmosphere, ocean, cryosphere and land applications, Elsevier, 2017.
[5] P. Tait, "High-resolution range profile," in Introduction to Radar Target Recognition, IET, 105–146 (2011).
[6] E. N. Fowle, E. J. Kelly, J. A. Sheehan, IRE Int. Convention record **4**, 136 (1961).
[7] P. M. Woodward, "Radar ambiguity analysis," 1967.
[8] A. W. Rihaczek, Proceedings of the IEEE **52**(2), 153 (1964).
[9] A. W. Rihaczek, Proceedings of the IEEE **53**(2), 116 (1965).
[10] A. W. Rihaczek, IEEE Transactions on Information Theory **13**(1), 51 (1967).
[11] L. J. Spafford, IEEE Transactions on Information Theory **14**(5), 734 (1968).
[12] H. Naparst, IEEE Transactions on Information Theory **37**(2), 317 (1991).
[13] V. C. Chen, H. Ling, Time Frequency Transforms for Radar Imaging and Signal Analysis, Artec House, MA, 98 (2002).
[14] M. Soumekh, Synthetic aperture radar signal processing with MATLAB algorithms, J. Wiley, NJ, 203 (1999).
[15] K. S. Chen, Principles of Synthetic Aperture Radar Imaging: A System Simulation Approach, CRC Press, FL **2**, 129 (2016).
[16] M. Martorella, Multidimensional Radar Imaging, The Institution of Engineering and Technology - Scitech Publishing, NC, 110 (2019).
[17] D. C. Munson, J. D. O'brien, W. K. Jenkins, Proceedings of the IEEE **71**(8), 917 (1983).
[18] A. W. Doerry, E. E. Bishop, J. A. Miller, Sandia National Laboratories Report, No. SAND 2016–1682 (2016).
[19] M. Soumekh, Algorithms for Synthetic Aperture Radar Imagery **3370**, 13 (1998).
[20] I. G. Cumming, Y. L. Neo, F. H. Wong, International Geoscience and Remote Sensing Symposium (IGARSS) **3**, 1455 (2003).
[21] A. Ribalta, IEEE Geoscience and Remote Sensing Letters **8**(3), 396 (2011).
[22] R. Lipps, D. Kerr, IEEE National Radar Conference – Proceedings 275 (1998).
[23] M. Vespe, G. Jones, C. J. Baker, Lessons for Radar, IEEE Signal Processing Magazine **26**(1), 65-75 (2009).
[24] W. G. Carrara, R. S. Goodman, R. M. Majewski, Spotlight Synthetic Aperture Radar: Signal Processing. Artech House Inc. MA, 225 (1995).
[25] Y. Huang, P. V. Brennan, D. Patrick, I. Weller, P. Roberts, K. Hughes, Progress in Electromagnetics Research **115**, 327 (2011).
[26] H. J. Visser, Array and phased array antenna basics. **2005**, J. Wiley, UK 79 (2005).
[27] R. C. Hansen, Phased array antennas, J. Wiley, NJ, 221 (2009).
[28] R. T. Lord, M. R. Inggs, High Range Resolution Radar using Narrowband Linear Chirps offset in frequency, Proc. IEEE South African Symp. on Communications and Signal Processing, COMSIG'97, Grahamstown, South Africa, pp. 9-12, September 1997.
[29] P. Swerling, IRE Transactions on Information Theory **6**(2), 269 (1960).
[30] C. S. Ku, K. S. Chen, P. C. Chang, Y. L. Chang, Remote Sensing **10**(9), 1404 (2018).
[31] N. Levanon, E. Mozeson, Radar Signals. Hoboken, John Wiley & Sons, Inc., NJ, USA, 63 (2004).
[32] B. R. Mahafza, Radar systems analysis and design using MATLAB. CRC Press, FL, 199 (2013).
[33] P. López-Rodríguez, R. Fernández-Recio, I. Bravo, A. Gardel, J. Lázaro, E. Rufo, Sensors **13**(4), 5381 (2013).

*Corresponding author: askind@sakarya.edu.tr